Similarities in the Phase Properties of Gibbs and Langmuir Monolayers

V. Melzer, D. Vollhardt,* G. Brezesinski, and H. Möhwald

Max-Planck-Institut für Kolloid- und Grenzflächenforschung, Berlin, Rudower Chaussee 5, D-12489 Berlin, Germany

Received: September 3, 1997; In Final Form: November 3, 1997[⊗]

A direct comparison of thermodynamical behavior and condensed-phase structures of adsorbed Gibbs monolayers with those of spread Langmuir monolayers of pure amphiphilic acid amide compounds at the air/water interface is presented. Thermodynamical behavior of adsorbed and spread monolayers of *N*-(γ-hydroxypropyl)tridecanoic acid amide (HTRAA) and *N*-(γ-hydroxypropyl)tetradecanoic acid amide (HTEAA) have been investigated with surface-pressure measurements ($\pi-A$ isotherms for HTRAA and HTEAA; $\pi-t$ adsorption kinetics for HTRAA). Those measurements were combined with Brewster angle microscopy (BAM) and synchrotron gracing incidence X-ray diffraction (GIXD) to study morphological features and crystal structures of the condensed phase. Adsorption kinetics and surface-pressure−area isotherms show a well-pronounced plateau region that starts at a characteristic inflection point. These characteristics are related to a first-order phase transition from a fluidlike to a condensed phase in the monolayers. A simple model enables the comparison of the adsorption kinetics with surface-pressure−area isotherms. Similar features of condensed phase domains are visualized by BAM for adsorbed and spread monolayers. Dendritic growth structures are found for all compounds and both types of monolayers. The molecules are arranged in an oblique lattice structure. The condensed phase structure is independent of the process of monolayer formation, but the density of defects is significantly smaller in the more homogeneously grown Gibbs monolayers.

Introduction

Processes of ordering and phase transitions as well as their effects on the thermodynamical behavior in two-dimensional systems have been of recent interest. Additionally, changes in the adsorption isotherms due to the phase transitions are important for practical applications. Emulsification, wetting, or sheathing processes will be distinctly influenced if phase transitions occur.

While phase transitions and structure formation in spread monolayers of water-insoluble molecules at the air/water interface (Langmuir monolayers) are well-studied,[1−4] in adsorption layers of water-soluble molecules (Gibbs monolayers) the first observation of such a phase transition has been reported and characterized very recently by using a special tailored amphiphile (*N*-dodecyl-γ-hydroxybutyric acid amide).[5−7]

To understand ordering processes in Gibbs monolayers and the effect of the phase transitions on the thermodynamical behavior, the question of a possible bridging between the structural properties of condensed phases in Gibbs and Langmuir monolayers arises.

Therefore, in the present work we focus on the comparison of phase behavior, morphologies, and crystal structures of adsorbed Gibbs monolayers with those of spread Langmuir monolayers of slightly water-soluble *N*-(γ-hydroxypropyl)-tridecanoic acid amide (HTRAA) and of water-insoluble *N*-(γ-hydroxypropyl)tetradecanoic acid amide (HTEAA). In both cases, the phase transition leads to the formation and the growth of two-dimensional condensed-phase domains. The features and growth of these domains can be visualized using Brewster angle microscopy (BAM). On the basis of the thermodynamical results, we will directly compare the adsorption kinetics with $\pi-A$ isotherms using a simple model, to understand the effect of the phase transition on the thermodynamical behavior of the monolayer during the adsorption process. The crystal structure of the condensed phases in Gibbs and Langmuir monolayers is investigated by using synchrotron gracing incidence X-ray diffraction (GIXD). GIXD enables one to investigate the arrangement of molecules on a molecular length scale. The condensed-phase structures of Gibbs and Langmuir monolayers will be compared to understand the ordering process of the molecules in the different types of monolayers.

Experimental Section

The slightly water-soluble surfactant *N*-(γ-hydroxypropyl)-tridecanoic acid amide (HTRAA) and the water-insoluble surfactant *N*-(γ-hydroxypropyl)tetradecanoic acid amide (HTEAA) were synthesized and purified following a procedure described for the C_{16} derivative elsewhere.[8] The surface-pressure (π)−area (A) isotherms and surface-pressure (π)−time (t) adsorption kinetics were recorded using a Langmuir film balance (R & K GmbH, Germany). Phase transitions in Gibbs monolayers were investigated for bulk concentrations between 0.7×10^{-5} mol/dm$^3 \leq c \leq 2 \times 10^{-5}$ mol/dm^3 in the temperature range between 4 and 20 °C. For more detailed information about the surface pressure measurements and the BAM method, see refs 5−7, 9, and 10. All presented BAM images show a section of the air/water interface with a vertical and horizontal size of 500 μm.

GIXD experiments[11−15] of the adsorbed HTRAA monolayer were performed at $T = 5$ °C and those of the spread monolayer of HTEAA at $T = 10$ °C, using the liquid−surface diffractometer on the undulator beam line BW1 at HASYLAB, DESY, Hamburg, Germany. The synchrotron beam was made monochromatic by a Beryllium (002) crystal and was adjusted to strike the surface at grazing incidence with an angle of incidence α_i

[⊗] Abstract published in *Advance ACS Abstracts,* December 15, 1997.

S1089-5647(97)02860-5 CCC: $15.00
Published on Web 01/15/1998

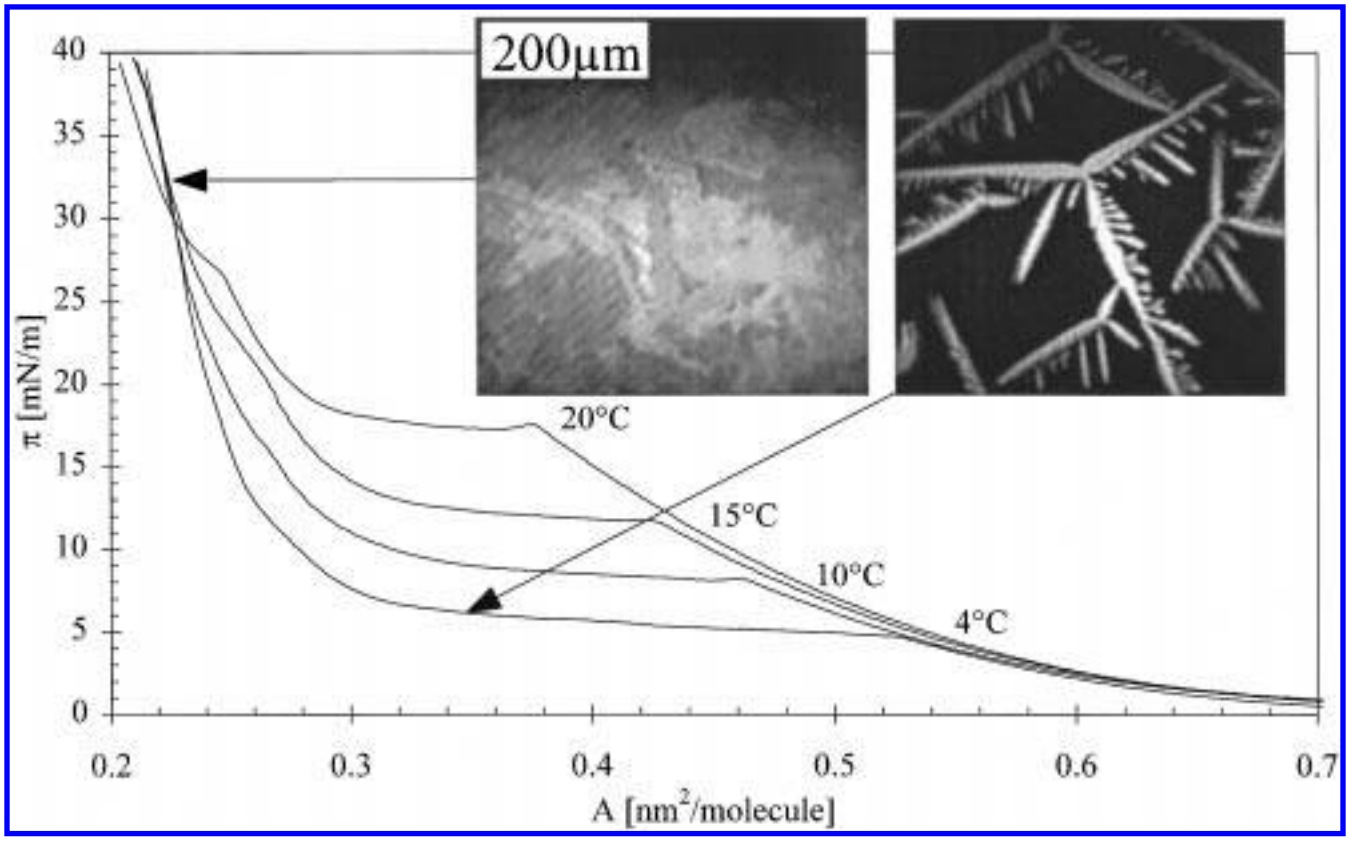

Figure 1. Pressure−area ($\pi-A$) isotherms of HTRAA at T = 4, 10, 15, and 20 °C. The characteristic BAM images of the HTRAA Langmuir monolayers, observed in the phase-transition region (right) and at higher lateral pressure (left), are inserted for T = 4 °C. The arrows indicate the positions where the BAM images were taken. The scale bar with a size of 200 μm is valid for all BAM images.

$= 0.85 \cdot \alpha_c$, where α_c is the critical angle for total external reflection. The diffracted radiation was detected by a linear position-sensitive detector (PSD) (OED-100-M, Braun, Garching, Germany) as a function of the vertical scattering angle α_f. A Soller collimator in front of the PSD provided resolution of the horizontal scattering angle $2\theta_{hor}$. Due to elastic scattering, the wave vectors $\mathbf{k}_i$ and $\mathbf{k}_f$ of the incident and the diffracted beam have the same modulus. The scattering vector $\mathbf{Q} = \mathbf{k}_f - \mathbf{k}_i$ has an in-plane component $Q_{xy} \approx (4\pi/\lambda)\cdot\sin(2\theta_{hor}/2)$ and an out-of-plane component $Q_z \approx (2\pi/\lambda)\cdot\sin(\alpha_f)$, where $\lambda = 1.364$ Å is the X-ray wavelength. The accumulated position-resolved scans were corrected for polarization, effective area, and powder averaging. The intensities were least-squares fitted by model peaks that were taken as the product of a Lorentzian parallel to the water surface with a Gaussian normal to it. Only the lowest order peaks are observed. To calculate the crystal structure (lattice spacings, unit cell area, tilt angle, and tilt direction of molecules), the obtained in-plane and out-of-plane diffraction data were analyzed according to the procedure described in refs 16−19. The GIXD measurements of the equilibrated Gibbs monolayer were started 3 h after the beginning of the phase transition (inflection point).

Results and Discussion

During the compression of the HTRAA Langmuir monolayer, a pronounced inflection point in the $\pi-A$ isotherm, followed by a plateau region, was observed. Such a plateau region is typical for a first-order phase transition from a low-density fluidlike to a condensed phase (Figure 1). The phase transition starts at the critical surface pressure π_c with the corresponding critical molecular area A_c. The critical surface pressure is temperature-dependent ($\Delta\pi_c/\Delta T = 0.9$ mN/m/K), and the size of the plateau region decreases with increasing temperature. The $\pi-A$ isotherms of HTRAA Langmuir monolayers were corrected for small loss of molecules into the subphase due to dissolution by a reasonable linear correction procedure as described in ref 6. Two typical BAM images of the HTRAA Langmuir monolayer are shown in Figure 1 to clarify the phase transition. These images confirm the coexistence of a fluidlike (dark regions) and a condensed phase (bright domains). The different tilt directions of the molecules in different domains can be seen by the different brightness. Typical domains exhibit from three to five dendritic main growth directions.

During the formation of an adsorbed Gibbs monolayer of HTRAA molecules, a pronounced inflection point is also observed in the $\pi-t$ adsorption isotherms at different temperatures (Figure 2). This conspicuous inflection point is related to a significant plateau region. At first, the surface pressure increases rapidly up to the critical surface pressure π_c. Above π_c, the surface pressure changes only weakly with time. Such a feature of the adsorption isotherm is typical for a first-order phase transition between a fluidlike and a condensed phase.[5−7] The dynamic adsorption process reaches an equilibrium state after a long time. The critical surface pressure of the phase transition increases with increasing temperature ($\Delta\pi_c/\Delta T = 0.9$ mN/m/K). Figure 2 shows two typical BAM images of the HTRAA Gibbs monolayer to illustrate the phase coexistence of a fluidlike and a condensed phase in the $\pi-t$ adsorption isotherm. The fluidlike phase is represented by dark regions and the condensed phase by bright domains. After a long time, the monolayer is almost completely transformed into the condensed state, and one can easily see the different tilt directions of the molecules in the different domains. It is also

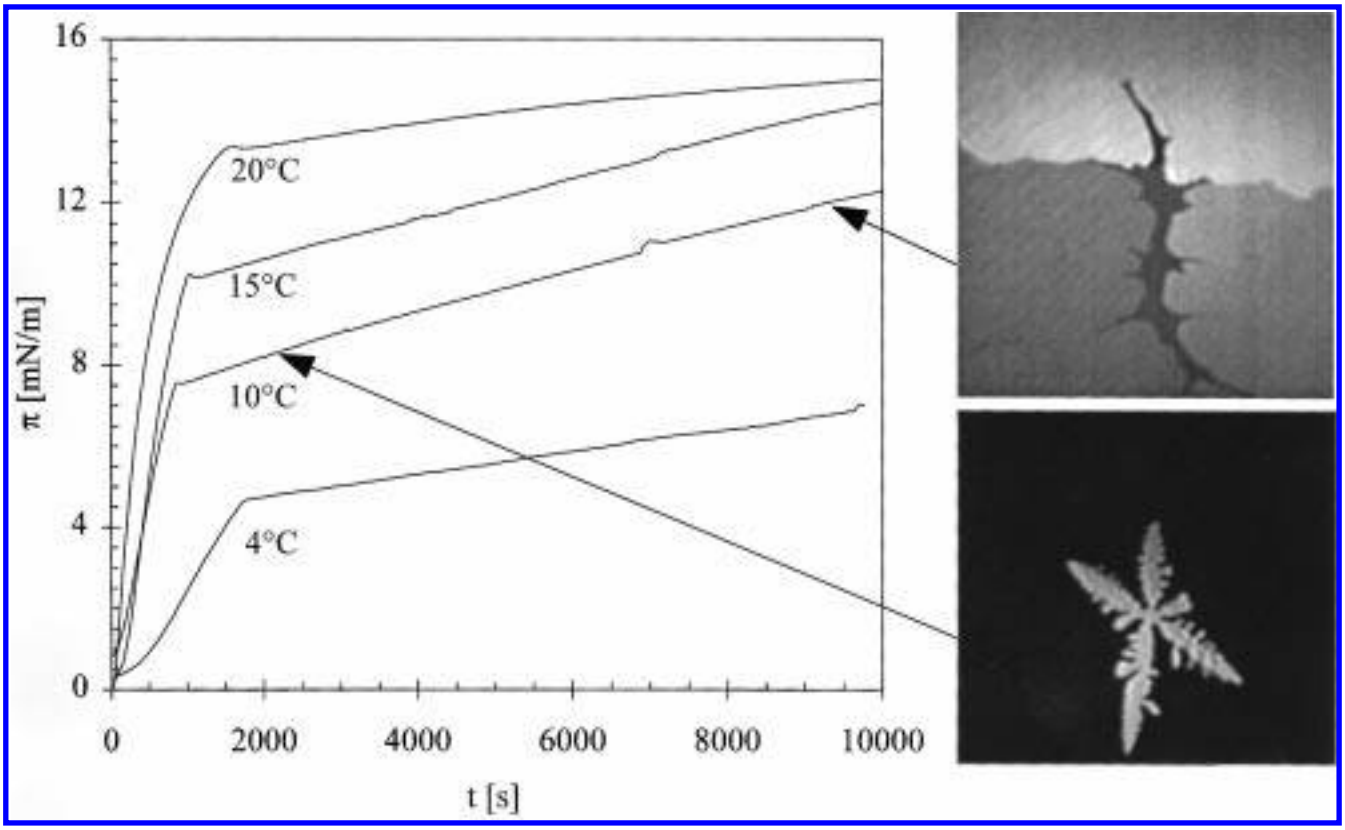

Figure 2. Pressure−time ($\pi-t$) adsorption kinetics of HTRAA at T = 4, 10, 15, and 20 °C at a bulk concentration of $c = 10^{-5}$ mol/dm^3. The characteristic BAM images of the HTRAA Gibbs monolayers in the two-phase coexistence region at T = 10 °C are inserted. The arrows indicate the times at which the BAM images were taken.

shown that the condensed-phase domains grow in several main growth directions.

The comparison between the $\pi-A$ and the adsorption isotherms and between the related BAM images (Figures 1 and 2) shows the similarities of the phase transitions and of the morphological features in the HTRAA monolayers. In both types of monolayers a conspicuous inflection point followed by a plateau region is observed. The critical phase-transition pressures and their temperature dependences are very similar. However, small but significant differences in the morphological features are observed. Due to the very slow and homogeneous growth process of condensed-phase domains in Gibbs monolayers, the tip shape of growing domains is broader compared to that in Langmuir monolayers. This is in good agreement with theoretical calculations that have shown that tip shape and tip splitting are related to the degree of deviation from equilibrium.[20,21] The much slower growth process is related to a more equilibrated state. The sizes of regions with the same gray values in the BAM images, which are regions of the same tilt orientation of the molecules, are also different. Hence, the orientational correlation length in the condensed-phase domains of Gibbs monolayers at the end of the phase-transition region is significantly larger compared to that of Langmuir monolayers (compare the BAM images in Figures 1 and 2). Therefore, the molecules can arrange in ordered structures with a lower density of defects during the adsorption process.

The similarities of phase transitions and morphological features of Gibbs and Langmuir monolayers enable a direct comparison between the $\pi-A$ and adsorption isotherms. We will try to answer this question by a transformation of the $\pi-t$ adsorption kinetics into a $\pi-A(t)$ adsorption kinetics, which can be directly compared with the $\pi-A$ isotherms. For this purpose one has to calculate the molecular area in dependence of adsorption time.

For the region below the critical surface pressure π_c, hence below t_c, an asymptotic solution of the Ward and Tordai equation[23] as the long-time approximation (eq 1)[22] of the adsorption kinetics can be used for the experimental times 20 s $\geq t \leq$ 7200 s in the fitting procedure

$$\Gamma(t) = \frac{2c\sqrt{\frac{DT}{\pi}}}{1 + 2\frac{dc}{d\Gamma}\sqrt{\frac{Dt}{\pi}}} \qquad (1)$$

where D is the diffusion coefficient and c the bulk concentration. For very long times, eq 1 converges to $\Gamma(t\rightarrow\infty) = c(dc/d\Gamma)^{-1}$. This is the fixed Γ value in equilibrium and can be calculated by using the adsorption isotherm $c = f(\Gamma)$. By using the relation $\Gamma = 1/(N_A A)$ between surface concentration Γ and molecular area A, which are related via Avogradro's number N_A, we obtain

$$A(t) = \frac{a_{ads}}{\sqrt{t}} + A_\infty \quad \text{with} \quad D = \frac{\pi N_A}{4c^2 a_{ads}^2} \quad \text{and} \quad \frac{dc}{d\Gamma} = \frac{A_\infty c}{N_A} \qquad (2)$$

In the simple eq 2, a_{ads} is an adsorption rate constant and A_∞ is the molecular area in the saturated state ($t = \infty$).

For each monolayer state there exists a correlation between the surface pressure and the molecular area. Hence we can directly correlate the $\pi-A$ isotherms with the adsorption kinetics in the region below π_c in which the monolayer is completely in a fluidlike state. The comparison of the surface pressures of the $\pi-A$ isotherms with those of the $\pi-t$ adsorption kinetics $\pi_{is}(A) = \pi_{ads}(t)$ results in a molecular area (A)−time (t)

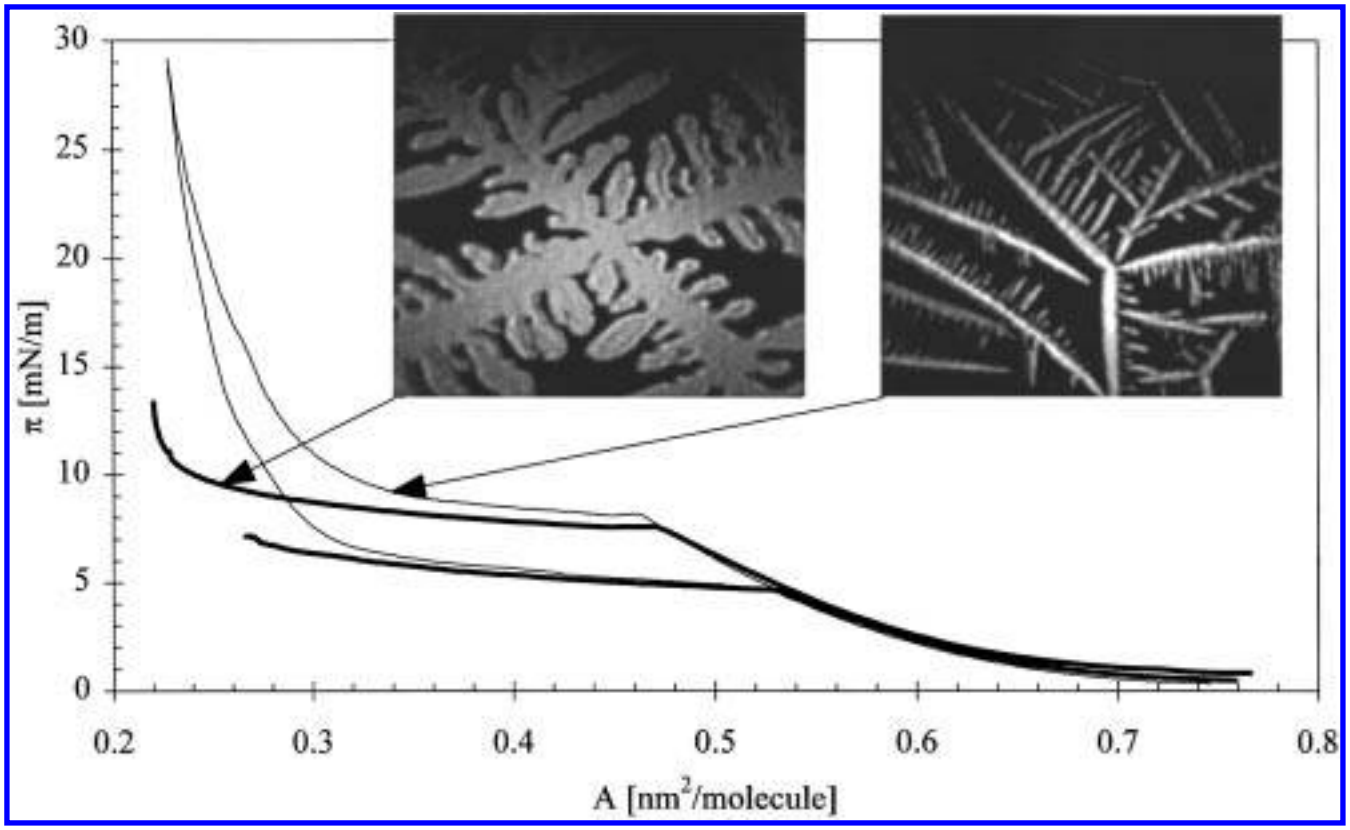

Figure 3. Comparison of $\pi-A$ isotherms (thin lines) and transformed $\pi-A(t)$ adsorption isotherms (thick lines) of HTRAA monolayers at T = 4 and 10 °C. Characteristic BAM images of the phase-coexistence region are inserted for Gibbs and Langmuir monolayers at T = 10 °C and π = 10 mN/m as indicated by the arrows.

correlation for the adsorbed monolayer. Consequently the molecular area in Gibbs monolayers during the adsorption process for times below t_c, i.e., before the phase transition starts, can be calculated. The obtained $A-t$ correlation can be conformed to eq 2. With these conformities, molecular areas A_∞ of the saturated state between 0.20 and 0.25 nm^2/molecule are obtained, which correspond to the molecular areas of the condensed phase in the $\pi-A$ isotherms (see Figure 3).

The long-time approximation for the adsorption kinetics (eq 1) is not valid for times above t_c due to the starting phase transition in the monolayer since then the process is no longer diffusion-controlled for the ordered phase. The reasonable assumption of a fixed molecular area of the fluidlike phase during the phase transition leads to a constant adsorption rate of molecules that adsorb only into regions of the fluidlike phase:

$$\frac{\mathrm{d}A}{\mathrm{d}t} = \text{const} = \frac{\mathrm{d}A(t_c)}{\mathrm{d}t} \quad \text{for} \quad t \geq t_c \tag{3}$$

In the phase coexistence region, the measured molecular area of the $\pi-A$ isotherms is an averaged value over the whole area of the surface ($F_0 = F_{LE} + F_{LC}$). F_{LE} is the area of the surface occupied by the fluidlike phase (with the molecular area A_{LE}), and F_{LC} is the area occupied by the condensed phase (with the molecular area A_{LC}); hence, for the averaged molecular area

$$A(t) = \frac{F_{LE}(t)}{F_0}(A_{LE} - A_{LC}) + A_{LC} \tag{4}$$

A small change of F_{LE} due to a small amount of freshly adsorbed molecules $\mathrm{d}N_{ads}$, with an adsorption rate as described by eq 3, is related to a small change of F_{LC}, because the adsorption leads to the transition to the condensed phase

$$-\mathrm{d}F_{LE} = A_{LC}\sum_{n=0}^{\infty}\left(\frac{A_{LC}}{A_{LE}}\right)^n \mathrm{d}N_{ads} = A_{LC}\frac{A_{LE}}{A_{LE} - A_{LC}}\mathrm{d}N_{ads} \tag{5}$$

On the other hand, a small change of F_{LC} is correlated to a small change of the averaged molecular area

$$A_{LC}\,\mathrm{d}N_{ads}(t) = -\frac{F_{LE}}{A_{LE}}\mathrm{d}A \tag{6}$$

Combination of eqs 3, 5, and 6 results in the simple differential equation

$$\mathrm{d}F_{LE} = \frac{\mathrm{d}A(t_c)}{\mathrm{d}t}\frac{F_{LE}}{A_{LE} - A_{LC}}\mathrm{d}t \tag{7}$$

Equation 7 can be directly integrated using the starting condition $F_{LE}(t_c) = F_0$

$$F_{LE}(t) = F_0 \exp\left(\frac{1}{A_{LE} - A_{LC}}\frac{\mathrm{d}A(t_c)}{\mathrm{d}t}(t - t_c)\right) \tag{8}$$

The combination of eqs 4 and 8 leads finally to

$$A(t) = (A_{LE} - A_{LC}) \exp\left(\frac{1}{A_{LE} - A_{LC}}\frac{\mathrm{d}A(t_c)}{\mathrm{d}t}(t - t_c)\right) + A_{LC} \tag{9}$$

This is the $A-t$ correlation for the adsorption kinetics. While eq 2 is valid for $t \leq t_c$, eq 9 must be used for $t \geq t_c$. At the critical point $t = t_c$, this function is continuous and differentiable. Hence the averaged molecular area changes continuously with time.

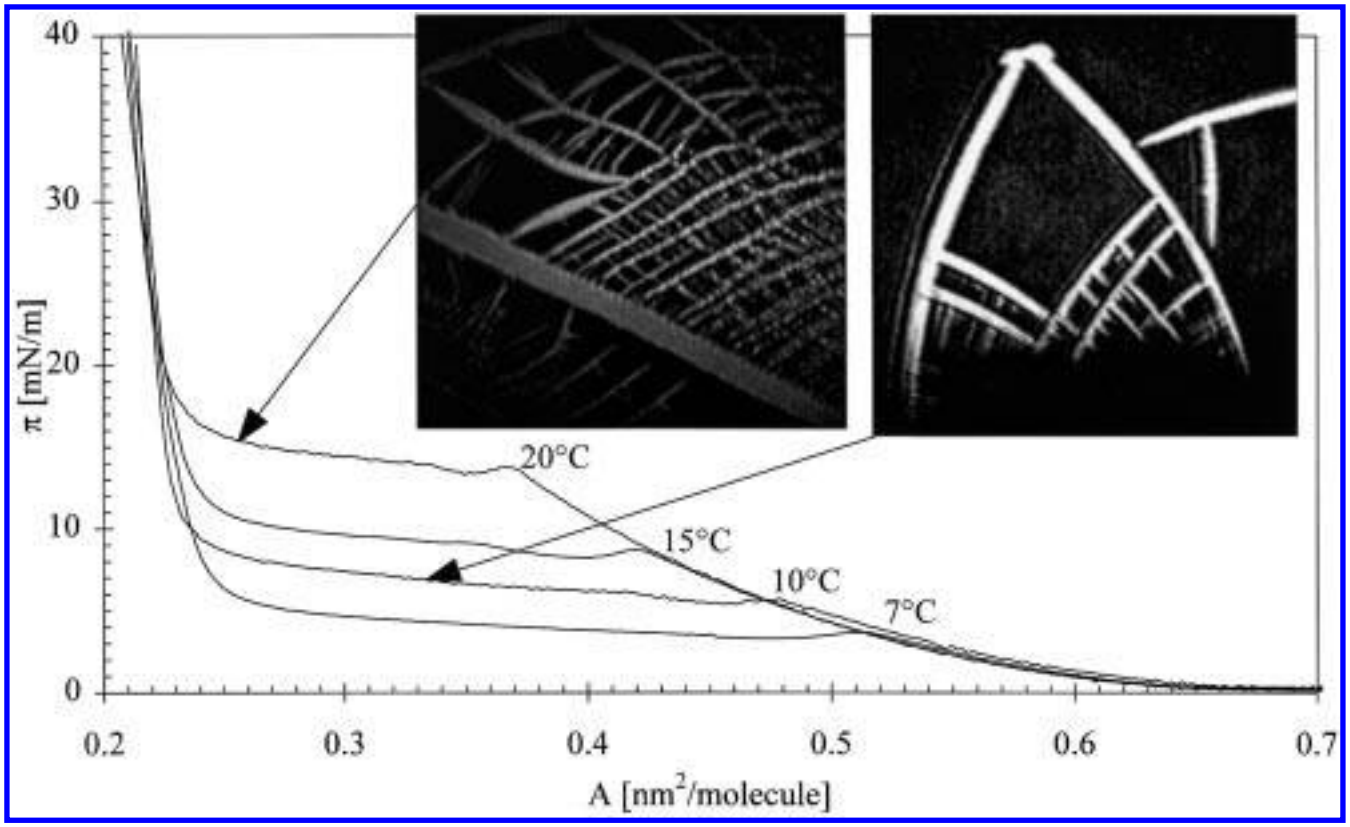

Figure 4. $\pi-A$ isotherms of HTEAA at T = 7, 10, 15, and 20 °C. The characteristic BAM images of the HTEAA Langmuir monolayers, observed in the phase-transition region, are inserted for T = 10 °C (right) and T = 20 °C (left). The arrows indicate the positions where the BAM images were taken.

The $\pi-A(t)$ adsorption isotherms can now be directly compared with the $\pi-A$ isotherms. The $\pi-A$ isotherms (Figure 1) and the $\pi-t$ adsorption kinetics (Figure 2) at T = 4 and 10 °C were used for the adjustment procedure to eq 2 and for the transformation of the $\pi-t$ adsorption kinetics by using eqs 2 and 9. The resulting curves are shown in Figure 3. The curves are identical before and at the beginning of the phase transition. However, the slopes deviate significantly for smaller molecular areas. This deviation is not unexpected. Due to the very slow and homogeneous adsorption process in the Gibbs monolayer, the deviations from the thermodynamical equilibrium are much smaller compared to those of the Langmuir monolayers. An ideal phase transition between two phases should exhibit a horizontal plateau region and two inflection points in the $\pi-A$ isotherms. Nonideal properties during the formation and the growth of two-dimensional condensed-phase aggregates[24] like kinetic effects between the molecules or aggregates lead to the increase in the surface pressure during the phase transition in the Langmuir monolayer and hence to a nonhorizontal plateau and to a completely smoothed second inflection point. These effects are much weaker in the slow phase-transition process in Gibbs monolayers. Therefore, the plateau region in such monolayers is closer to an ideal behavior, what is also supported by the broader morphological features of domains, grown in Gibbs monolayers, compared to those of Langmuir monolayers (see BAM images in Figure 3). The phase-transition pressures of adsorption isotherms are always slightly below the phase-transition pressures of $\pi-A$ isotherms (Figure 3) due to the smaller deviation from equilibrium in Gibbs monolayers.

The crystal structures of condensed phases in Gibbs and Langmuir monolayers are measured using GIXD. The Gibbs monolayers of HTRAA form long-time stable condensed-phase structures. Because of the dissolution process in Langmuir monolayers of the slightly water-soluble HTRAA molecules, the water-insoluble HTEAA molecules were used for the GIXD measurements. These molecules have the same headgroup structure but a slightly elongated alkyl chain (one additional methylene group). Langmuir monolayers of these molecules are long-time stable at the air/water interface. The increase of the alkyl chain length leads to a decrease of the critical phase-transition pressure at a constant temperature.[25] The $\pi-A$ isotherms of HTEAA Langmuir monolayers are shown in Figure 4. One can easily see the expected plateau region with the lowered critical phase-transition pressure compared to HTRAA Langmuir monolayers (compare Figure 1 with Figure 4). The inserted BAM images taken in the phase-coexistence region demonstrate the similar dendritic growth structures of HTRAA and HTEAA monolayers. The obvious similarities in the thermodynamical behavior and morphological features between HTEAA and HTRAA monolayers allow the comparison of the condensed-phase structures in Langmuir monolayers of HTEAA and in Gibbs monolayers of HTRAA.

The contour plots of the Gibbs monolayer of HTRAA and the Langmuir monolayer of HTEAA are presented in Figure 5 for different surface pressures. The peak maxima and their full widths at half-maximum (fwhm) of the in-plane (Q_{xy}, ΔQ_{xy}) and the out-of-plane (Q_z, ΔQ_z) scattering vector components are listed in Table 1.

The indexing of the diffraction peaks, which was used for the calculation of the lattice parameters, is marked in the contour plots (Figure 5). The same indexing of the diffraction peaks was used for Gibbs and Langmuir monolayers. This seems to be reasonable due to the obviously comparable positions of the diffraction peaks. It is important to note that the fwhm of the in-plane (10) diffraction peak is resolution-limited for both types of monolayer at all surface pressures investigated. Additionally,

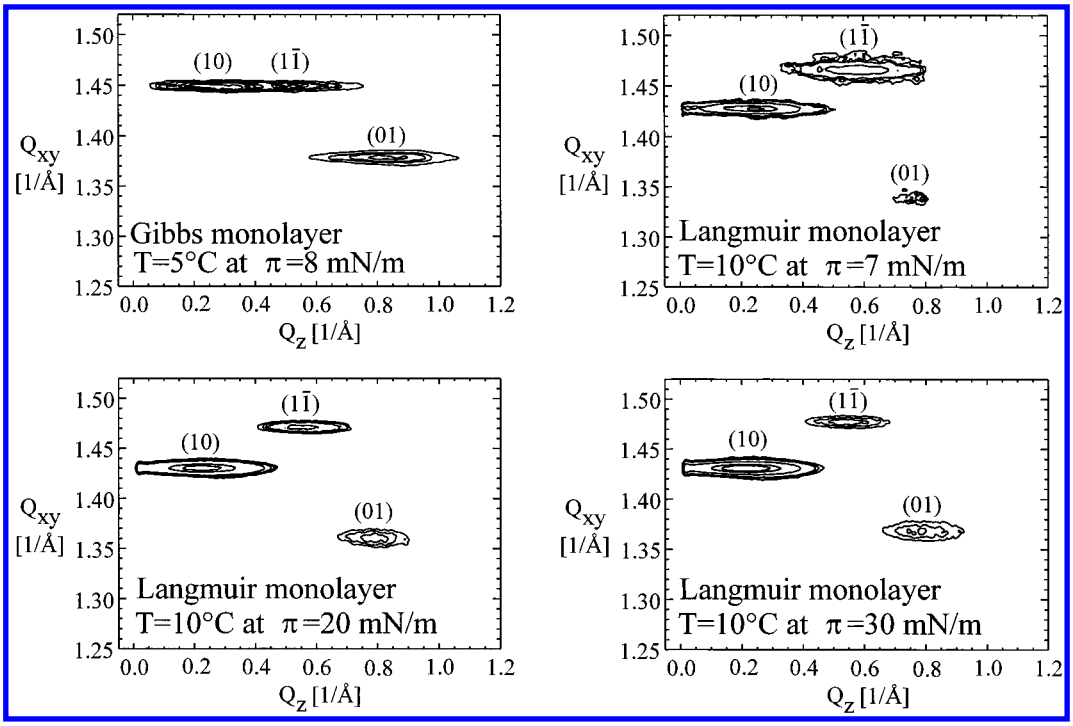

Figure 5. Contour plots of the HTRAA Gibbs monolayer ($c = 10^{-5}$ mol/dm^3, $T = 5$ °C, $\pi = 8$ mN/m) and of the HTEAA Langmuir monolayer ($T = 10$ °C, $\pi = 7$, 20, 30 mN/m). The indexes of the diffraction peaks are given above the corresponding peaks.

TABLE 1: Maxima (Q_{xy} and Q_z) and Full Width at Half-Maximum (ΔQ_{xy} and ΔQ_z) of the Diffraction Peaks[a] of the HTRAA Gibbs Monolayer and of the HTEAA Langmuir Monolayer at Different Surface Pressures

π [mN/m]	Q_{xy} (ΔQ_{xy}) (10) [1/Å]	Q_z (ΔQ_z) (10) [1/Å]	Q_{xy} (ΔQ_{xy}) (01) [1/Å]	Q_z (ΔQ_z) (01) [1/Å]	Q_{xy} (ΔQ_{xy}) (11) [1/Å]	Q_z (ΔQ_z) (11) [1/Å]
			HTRAA at $T = 5$ °C			
8	1.450	0.29	1.379	0.85	1.450	0.56
	(0.006)	(0.24)	(0.008)	(0.30)	(0.008)	(0.18)
			HTEAA at $T = 10$ °C			
7	1.427	0.26	1.339	0.85	1.466	0.60
	(0.007)	(0.21)	(0.016)	(0.29)	(0.011)	(0.30)
20	1.430	0.24	1.360	0.82	1.471	0.59
	(0.008)	(0.24)	(0.027)	(0.25)	(0.013)	(0.29)
30	1.431	0.22	1.368	0.79	1.478	0.57
	(0.009)	(0.25)	(0.028)	(0.31)	(0.015)	(0.27)

[a] Q_{xy}, in-plane component, and Q_z, out-of-plane component, of the scattering vector.

TABLE 2: Lattice Parameters of the Condensed Phases in HTRAA Gibbs Monolayers and in HTEAA Langmuir Monolayers at Different Surface Pressures[a]

π [mN/m]	a [Å]	b [Å]	c [Å]	A_{xy} [Å^2]	A_0 [Å^2]	γ [deg]	ψ_a [deg]	τ [deg]
				HTRAA at $T = 5$ °C				
8	4.926	5.179	5.181	22.5	19.0	118.4	99.8	32.0
				HTEAA at $T = 10$ °C				
7	4.901	5.225	5.366	23.0	19.3	116.1	100.0	32.9
20	4.905	5.158	5.306	22.7	19.3	116.4	100.6	31.4
30	4.898	5.123	5.290	22.5	19.4	116.3	100.8	30.5

[a] a, b, c, lattice spacings; γ, angle between [10] direction (a) and [01] direction (b); A_{xy}, molecular area parallel to the interface; τ, polar tilt angle of the molecules; A_0, cross-sectional area per alkyl chain perpendicular to the chain axis; ψ_a, azimuthal tilt angle of molecules according to the [10] direction (a).

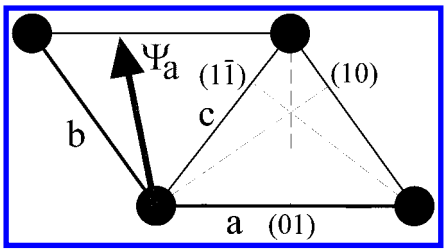

Figure 6. Model of the crystal structure of an oblique lattice observed in Gibbs and Langmuir monolayers. Positions of the molecules are presented by filled circles. The gray arrow symbolizes the azimuthal tilt direction of the molecules. Additionally the lattice spacings (dashed lines) are indicated.

all other diffraction peaks of the HTRAA Gibbs monolayer are also resolution-limited, whereas in the case of the HTEAA Langmuir monolayer the fwhm of the other peaks is well above the resolution limit of $\Delta Q_{xy} = 0.008$ Å^{-1}. Hence, the positional correlation length of the condensed-phase structure is significantly larger in the Gibbs monolayer compared to that in the Langmuir monolayer. This is in good agreement with the slower and more homogeneous growth process of the condensed phase in the adsorption layer.

The lattice parameters of the condensed phases of the two monolayers are listed in Table 2. The condensed phases of HTRAA and HTEAA monolayers exhibit a very similar oblique lattice structure with large unit cell areas ($A_{xy} > 22$ Å^2) and large tilt angles of the molecules ($\tau > 30°$). The tilt direction of the alkyl chains is nearly parallel to the [13] direction ($\psi_a \approx 100°$). Figure 6 shows a sketch of the lattice structure. The tilt angles and lattice parameters change only slightly with increasing surface pressure; therefore, rigid hydrogen-bondings between the amide groups can be assumed.

The observed diffraction peaks and structure similarities between the Gibbs and Langmuir monolayers are additional evidence for the phase transition and the formation of a condensed phase in the Gibbs monolayer. Neither in the Gibbs nor in the Langmuir monolayer could three-dimensional clusters or aggregates be observed (Figure 5).

The density of lattice defects is low parallel to the direction of a directed bond.[26] The dependence of the lattice spacings on the lateral pressure must be also significantly smaller parallel to this directed bond. Therefore, it can be assumed that the hydrogen bonds formed between the acid amid groups are parallel to the lattice line a (Table 2 and Figure 6). This is in good agreement with the three-dimensional crystal structure of a similar amphiphilic acid amide compound[8] that has only a more elongated alkyl chain. A comparison of the found lattice structure with similar oblique lattices of monolayers formed by similar acid amide compounds is also of interest.[18,19]

The observed dendritic growth is related to the influence of anisotropy of the directed hydrogen bonds between the acid amide groups. While van der Waals interactions between alkyl chains are isotropic, resulting in a nondirected compact growth as observed for fatty acids[27] and fatty alcohols,[28] the strong dipole−dipole interactions between the acid amide groups determine the dendritic growth of the condensed-phase domains in preferred directions.[29]

Conclusions

In summary, evidence has been provided for a first-order phase transition for adsorbed monolayers of HTRAA and for spread monolayers of HTRAA and HTEAA. The phase transition was visualized using Brewster angle microscopy. By using a simple model for the calculation of the molecular area in dependence of the adsorption time, the $\pi-t$ adsorption isotherms can be directly compared with $\pi-A$ isotherms. This comparison shows the similarities in the thermodynamical behavior of Gibbs and Langmuir monolayers and the differences due to a more equilibrated growth of the Gibbs monolayers.

The condensed phase structures were analyzed using grazing incidence X-ray diffraction at the air/water interface. The oblique crystal structure was independent of the process of monolayer formation, but the density of defects was significantly smaller in Gibbs monolayers compared to that in Langmuir monolayers. It has been shown that in HTRAA and HTEAA monolayers strong hydrogen bonds between acid amid groups enable additional attractive interactions, which have a significant effect on the formation of dendritic condensed monolayer phase domains.

Acknowledgment. Financial assistance from the Deutsche Forschungsgemeinschaft (SFB 312 “Gerichtete Membranprozesse”) and the Max-Planck-Institut für Kolloid- und Grenzflächenforschung is gratefully acknowledged. We thank Dr. G. Weidemann for valuable discussions, Dr. R. Wagner for preparing the amphiphiles, and HASYLAB at DESY for providing excellent facilities and support.

References and Notes

(1) Gaines, G. L. In *Insoluble Monolayers at Liquid−Gas Interfaces*; Interscience: New York, 1966.
(2) Knobler, C. M. *Science* **1990**, *240*, 870.
(3) Möhwald, H. *Rep. Prog. Phys.* **1993**, *56*, 653.
(4) Vollhardt, D. *Adv. Colloid Interface Sci.* **1996**, *64*, 143.
(5) Melzer, V.; Vollhardt, D. *Phys. Rev. Lett.* **1996**, *76*, 3770.
(6) Melzer, V.; Vollhardt, D. *Prog. Colloid. Polym. Sci.* **1997**, *105* 130.
(7) Vollhardt, D.; Melzer, V. *J. Phys. Chem. B* **1997**, *101*, 3370.
(8) Rudert, R.; Wu, Y.; Vollhardt, D. *Z. Kristallogr.* **1996**, *211*, 114.
(9) Hönig, D.; Möbius, D. *J. Phys. Chem.* **1991**, *95*, 4590.
(10) Hénon, S.; Meunier, J. *Rev. Sci. Instrum.* **1991**, *62*, 936.
(11) Als-Nielsen, J. In *Structure and Dynamics of Surfaces*; Schommers, W., von Blanckenhagen P., Eds.; Springer-Verlag: Berlin, 1986; Vol. 2.
(12) Als-Nielsen, J.; Kjaer, K. In *Phase Transitions in Soft Condensed Matter*; Riste, T., Sherrington, D., Eds.; NATO ASI Series B; Plenum Press: New York, 1989.
(13) Kjaer, K. *Physica B* **1994**, *198*, 100.
(14) Als-Nielsen, J.; Jaquemain, D.; Kjaer, K.; Lahav, M.; Leveiller, F.; Leiserowitz, L. *Phys. Rep.* **1994**, *246*, 251.
(15) Als-Nielsen, J.; Möhwald, H. In *Handbook on Synchrotron Radiation*; Ebrashi, S., Koch, M., Rubenstein, E.; Eds.; Elsevier Science Publishers B.V.: Amsterdam, 1991.
(16) Brezesinski, G.; Scalas, E.; Struth, B.; Möhwald, H.; Bringezu, F.; Gehlert, U.; Weidemann, G.; Vollhardt, D. *J. Phys. Chem.* **1995**, *99*, 8758.
(17) Gehlert, U.; Vollhardt, D.; Brezesinski, G.; Möhwald, H. *Langmuir* **1996**, *12*, 4892.
(18) Melzer, V.; Weidemann, G.; Vollhardt, D.; Brezesinski, G.; Wagner, R.; Struth, B.; Möhwald, H. *J. Phys. Chem. B* **1997**, *101*, 4752.
(19) Melzer, V.; Weidemann, G.; Vollhardt, D.; Brezesinski, G.; Wagner, R.; Struth, B.; Möhwald, H. *Supramol. Sci.*, in press.
(20) Gliozzi, A.; Levi, A. C.; Menessini, M.; Scalas, E. *Physica A* **1994**, *203*, 347.
(21) Indiveri, G.; Levi, A. C.; Gliozzi, A.; Scalas, E.; Möhwald, H. *Thin Solid Films* **1996**, *284/285*, 106.
(22) Rillaertes, E.; Joos, P. *J. Phys. Chem.* **1982**, *86*, 3471.
(23) Ward, A. F. H.; Tordai, L. *J. Chem. Phys.* **1946**, *14*, 453.
(24) Fainerman, V. B.; Vollhardt, D.; Melzer, V. *J. Phys. Chem.* **1996**, *100*, 15478.
(25) Adam, N. K. *Proc. R. Soc. London* **1922**, *A101*, 522.
(26) Weinbach, S. P.; Jacquemain, D.; Leveiller, F.; Kjaer, K.; Als-Nielsen, J.; Leiserowitz, L. J *J. Am. Chem. Soc.* **1993**, *115*, 11110.
(27) Knobler, C. M. *Adv. Chem. Phys.* **1990**, *77*, 397.
(28) Siegel, S.; Vollhardt, D. *Prog. Colloid. Polym. Sci.* **1994**, *97*, 16.
(29) Melzer, V.; Vollhardt, D.; Weidemann, G.; Brezesinski, G.; Wagner, R.; Möhwald, H. *Phys. Rev. E*, in press.